

# Analytical Study on Shear Resistance of Beam-Column Joints Composed of Ultra High Strength Concrete Containing Steel Fiber



**H. Noguchi**

*Kogakuin University, Tokyo, Japan*

**T. Kashiwazaki**

*Chiba University, Chiba, Japan*

**H. Takatsu & H. Kimura**

*Takenaka Corporation, Chiba, Japan*

## **ABSTRACT:**

Three-dimensional finite element method (FEM) analysis was performed using the steel fiber and beam width as variables on beam-column joints composed of ultra high strength concrete containing steel fiber (Fc150). Adding steel fiber to concrete improves the effective width and the shear strength of a beam-column joint based on the AIJ Design Guidelines [9] for Earthquake Resistant Reinforced Concrete Buildings Based on Inelastic Displacement Concept as well as the shear resistance of the beam-column joint. Moreover, adding steel fiber changes the stress distribution at the critical cross-section of the beam and reduces the proportion of shear force applied to the joint by the bond force of the main beam reinforcement.

*Keywords: ultra high strength concrete, steel fiber, beam-column joint, finite element method, shear strength*

## **1. INTRODUCTION**

Concrete with a design strength of  $100 \text{ N/mm}^2$  has practical applications in reinforced concrete (RC) used in super high-rise buildings. However, a vast amount of lateral reinforcement may be required to satisfy design criteria, and there may be instances in which reinforcement is unrealistic. To resolve this issue, ultra high strength concrete containing steel fiber (SF) is being developed and applied to actual designs with the goal of reducing the amount of reinforcement and controlling crack damage in concrete. Takatsu et al. (2009), Takahashi et al. (2009), and Sakashita et al. (2010) have reported an increase in the shear resistance of beam-column joints using ultra high strength concrete containing SF. In this study, 3-D FEM analysis was performed to examine the causes and mechanisms behind the increase in shear resistance of beam-column joints due to the addition of SF.

## **2. ANALYSIS OVERVIEW**

### **2.1. Test specimens**

The specimens in this study are the same as those used in the experiment performed by Takatsu et al. (2009). Figure 1 shows the experimental specimen. Force was applied to the specimen via displacement control using jacks installed at both ends of the beam, and a constant axial force with a compressive axial force ratio of 0.01 was introduced to the column.

Herein the variable factors, beam width (152.5 mm and 250 mm) and SF content (0.0%, 0.5%, 1.0%, and 1.5%) were extended in the analysis. However, the beam width was 250 mm in the experiment where the SF content varied (0.0%, 0.5%, and 1.0%). Table 1 lists the test specimens. First the material characteristics and other concrete properties were compared to the test specimens. Then the model, which is described below, was used to verify the maximum resistance and initial stiffness were consistent between the experimental and analytical results. Next analyses were conducted to elucidate only the effect of adding SF by analyzing the characteristics and properties of concrete equal to

specimen J150-0.0 (without added SF). Additionally, the 152.5-N series, which contains imaginary specimens, was analyzed using the same amount of reinforcements as the 250-N series. Table 2 lists the common properties of all specimens.

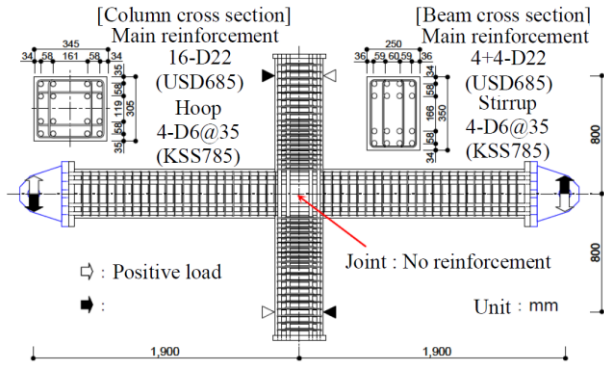


Figure 1: Test specimen

Table 1: Test specimens

Test specimens	Beam width	SF mixing amount	(Region of tension stiffening) Parameter c of Morita-Kaku model
250-N-0.0	250 (mm)	0.0%	1.00
250-N-0.5		0.5%	0.23
250-N-1.0		1.0%	0.14
250-N-1.5		1.5%	0.01
152.5-N-0.0	152.5 (mm)	0.0%	1.00
152.5-N-0.5		0.5%	0.23
152.5-N-1.0		1.0%	0.14
152.5-N-1.5		1.5%	0.01

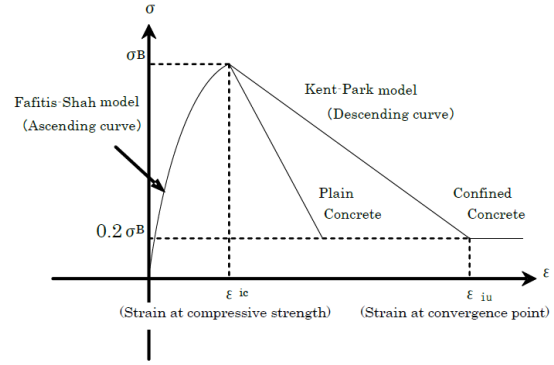


Fig. 2: Material characteristics of concrete

Table 2: Common properties for all specimens

Concrete compressive strength (N/mm <sup>2</sup> )	144.6
Concrete Young's modulus (N/mm <sup>2</sup> )	4.09×10 <sup>4</sup>
Main reinforcement yield strength (N/mm <sup>2</sup> )	714.4
Main reinforcement Young's modulus (N/mm <sup>2</sup> )	1.96×10 <sup>5</sup>
Lateral reinforcement yield strength (N/mm <sup>2</sup> )	984.8
Lateral reinforcement Young's modulus (N/mm <sup>2</sup> )	1.96×10 <sup>5</sup>
Main reinforcement arrangement	4+4-D22 (USD685)
Lateral reinforcement arrangement	4-D6@35 (KSS785)

## 2.2. Analytical models

### 2.2.1. Concrete

In the present study, we used a three-dimensional FEM analysis program developed by Yo and Noguchi et al. (2005) and refined by Hong et al. (2009). The concrete was expressed using isoparametric eight-node solid elements. A model, in which Darwin–Pecknold's orthotropic hypo-elastic model based on equivalent uniaxial strain is expanded to three dimensions, was used for the constitutive law. The five-parameter model by experiment by Kupfer *et al.*, was used for the failure curve. The stress–strain relationship was evaluated according to location. The Fafitis–Shah equation, which corresponds to the high strength concrete used in the present study, was used to assess the ascending section on the compression side, while the Kent–Park equation, which considers the restraining effect of the lateral reinforcements, was used for the descending section. Figure 2 shows the material characteristics of concrete. The Iizuka equation, in which the compression strength is reduced when strain is increased in the direction orthogonal to the crack direction, was used as the compressive strength reduction factor. The orthogonal fixed crack model was used as the crack model, while the Al–Mahaidi model was used to express the shear transmission characteristics in the crack direction. The Shirai equation was used to model the tension-softening region for specimens lacking SF, but the tension-softening region was estimated using from the existing data in a reference by Kobayashi et al. (1980) as well as our results of a reinforcement pull-out test for ultra high strength concrete containing SF. The Morita–Kaku model was used to account for the effect of SF addition where the parameter c for Fc150 was 0.23, 0.14, and 0.01 for 0.5%, 1.0%, and 1.5% SF content, respectively. Figure 3 models the tension-softening region. See a reference by Sekiguchi et al. (2010) for a discussion about the model.

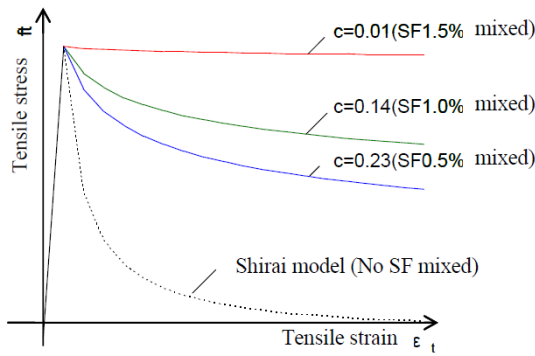


Fig. 3: Modelling of tension stiffening region

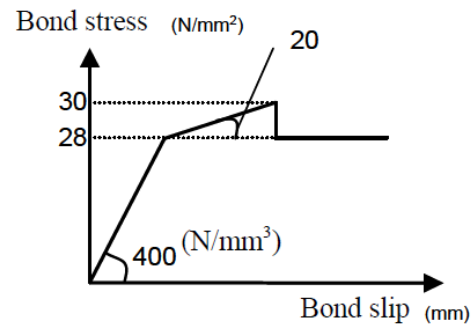


Fig. 4: Bond characteristics

### 2.2.2. Reinforcement

Two-node linear elements, which only consider axial-direction stiffness, were used to express the reinforcements. A modified Menegotto–Pinto model was used to model the stress–strain relationship.

### 2.2.3. Bond

Figure 4 shows the bond characteristics, which were established using the bond stress obtained from a reference by Tsuji et al. (2008) as the bond stress at the second bend point.

## 2.3. A finite element idealization and boundary conditions

Figure 5 show the finite element idealization and boundary conditions while applying a story shear force for the 250-N series. For finite element idealization, the test specimen was split in half in the y-axis direction due to symmetry with the cutting surface restrained in the y-axis direction. Similar to the experiment, for the boundary conditions to apply to a story shear force, force was applied to the center row at the beam ends using displacement control. To restrain the column while determining the story shear force and after considering column rotation, the center row was restrained in the x-axis direction (when the cutting surface was restrained in the x- and y-axis directions) for the upper reaction force point, and in the x- and z-axis directions (where the cutting surface was restrained in the x-, y-, and z-axis directions) for the lower reaction force point. Element discretization and boundary conditions were similar for the 152.5-N series.

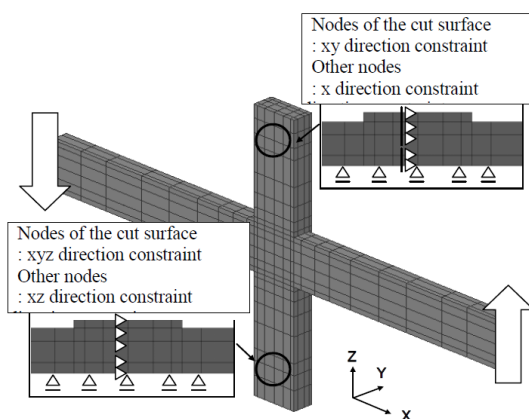


Fig. 5: Finite element idealization and boundary conditions

Table 3: Comparison of story shear resistances

250-N series		
SF mixing amount (%)	Vc max (kN)	Vc growth rate
0.0	500	1.00
0.5	552	1.10
1.0	572	1.14
1.5	614	1.23
152.5-N series		
0.0	334	1.00
0.5	413	1.24
1.0	456	1.37
1.5	510	1.53

### 3. ANALYTICAL RESULTS

#### 3.1. Story shear force–story drift angle relationship

Figure 6 shows the relationship between the story shear force and the story drift angle. The upper row compares the experimental and analytical values where the material characteristics and other properties of the concrete are experimental values. The analytical values have a low stiffness in 250-N-0.0, and a low maximum resistance in 250-N-1.0. However, because the trends of the hysteresis loops correspond well between the experiment and the analysis, improving the tension-softening region allows the effect of adding SF to be satisfactorily reproduced. The lower row compares the material characteristics and other properties shown in Table 2. Table 3 compares the story shear resistance, which increases by a maximum of 1.23% and 1.53% in the 250-N and 152.5-N series, respectively. (Both represent instances in which 1.5% SF was added.) The increase in resistance is greater in the 152.5-N series than in the 250-N series.

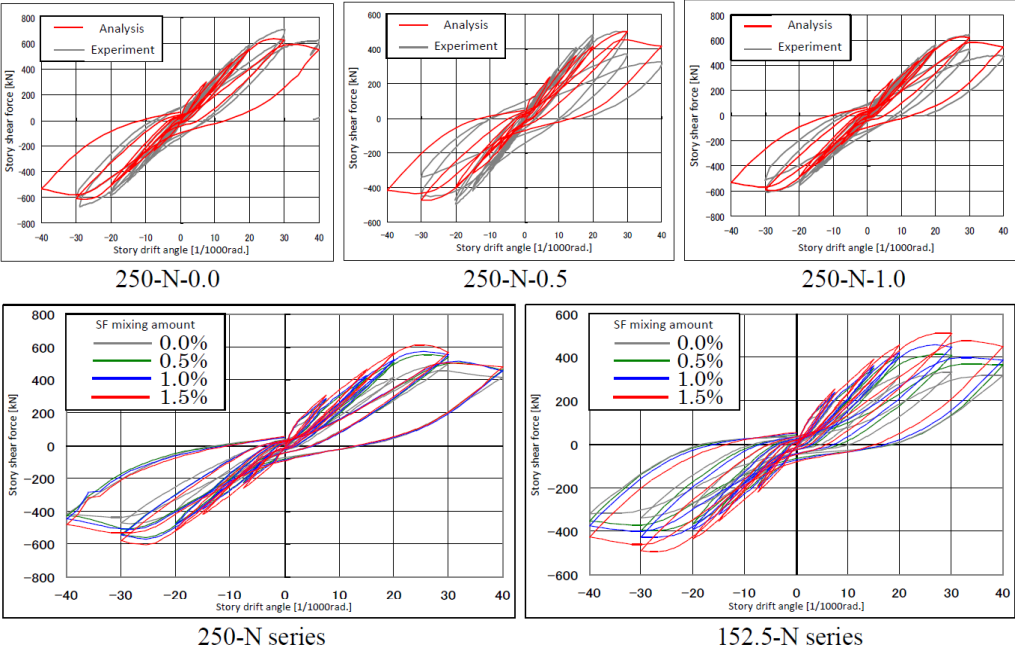


Fig. 6: Relationship between story shear force and story drift angle

#### 3.2. Joint input shear force–joint shear drift angle relationship

Figure 7 shows the relationship between the joint input shear force and the joint shear drift angle. The joint shear drift angle was calculated from the displacement of the nodes at the four corners of the joint panel, and the joint input shear force was calculated using the AIJ Design Guidelines (1999). The diagrams also show the joint shear strengths obtained from the AIJ Design Guidelines ( $\phi=1.0, 0.85$ ). For both series, if the design equation in the AIJ Design Guidelines does not indicate a danger, the addition of SF is deemed to be safe. Moreover, the addition of SF inhibits shear deformation of the joint, and this phenomenon is particularly prominent in the 152.5-N series.

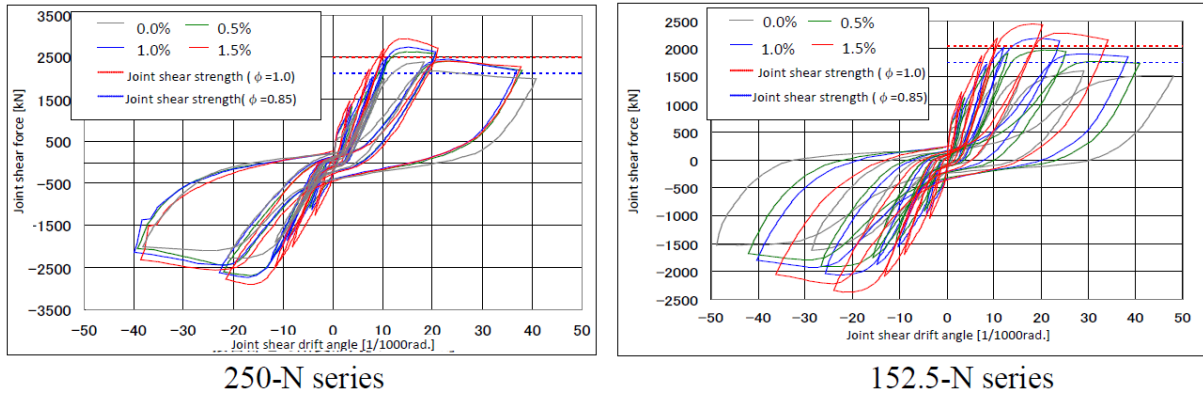


Fig. 7: Relationship between joint shear force and joint shear drift angle

### 3.3. Minimum principle strain distribution in the joint

Figure 8 shows the elements in the minimum principle strain measurements. The values measured using elements within the compressive strut regions shown in (a) the vertical cross-section are represented as a distribution in the column-width direction in (b) the horizontal cross-section. Figure 9 shows the minimum principle strain distribution in the joint when the story drift angle is 20/1000 rad. and 30/1000 rad.. When the story drift angle is 20/1000 rad., the minimum principle strain development is relatively low near the concrete surface for specimens in both series without SF. For specimens containing SF, the minimum principle strain in the concrete surface develops in a similar manner as other elements. In other words, the addition of SF causes compressive deformation transmitted as compressive struts to occur across the whole column-width direction in the joint. Additionally, the development of minimum principle strain is prominent in elements where the maximum principle strain is significant (shown further below). This effect remains small for 250-N series specimens with a SF content of 1.0% or more. When the story drift angle is 30/1000 rad., the minimum principle strain exceeds the strain at the concrete compressive strength ( $\epsilon_{cb} = -4400[\mu]$ ) for all specimens. Therefore, all specimens have experienced joint shear failure.

### 3.4. Maximum principle strain distribution in the joint

The elements for the maximum principle strain measurements and distribution direction are the same as those for the compressive principle strain in the joints (Figure 8). Figure 10 shows the maximum principle strain distribution in the joints when the story drift angle is 20/1000 rad.. For both series, specimens without SF have elements with a localized increase in the maximum principle strain. However, the addition of SF inhibits the localized increase. In other words, the addition of SF inhibits localization of compressive characteristics degradation caused by concrete cracking.

### 3.5. Compressive principle stress distribution in the joint

Compressive principle stress measurement elements and the distribution direction are the same as those for the compressive principle strain in the joints (Figure 8). Figure 11 shows the compressive principle stress distribution when the story drift angle is 20/1000 rad.. In both series, the addition of SF causes a uniform distribution of the compressive stress across the entire column-width direction. This is due to the addition of SF and the uniform distribution of the minimum principle strain, which cause compressive deformation to be transmitted as compressive struts across the entire column-width direction, as shown in 3.3, and inhibition of localization of compressive characteristic degradation caused by concrete cracking, as shown in 3.4. Therefore, the addition of SF increases the effective cross-section area of the compressive struts in the direction of column width.

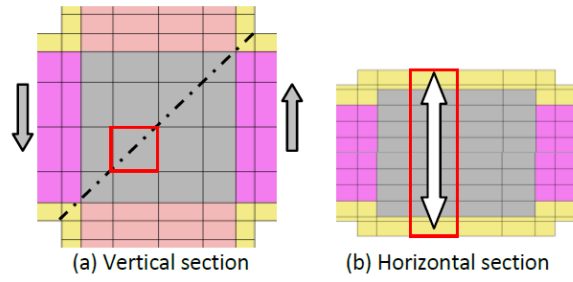
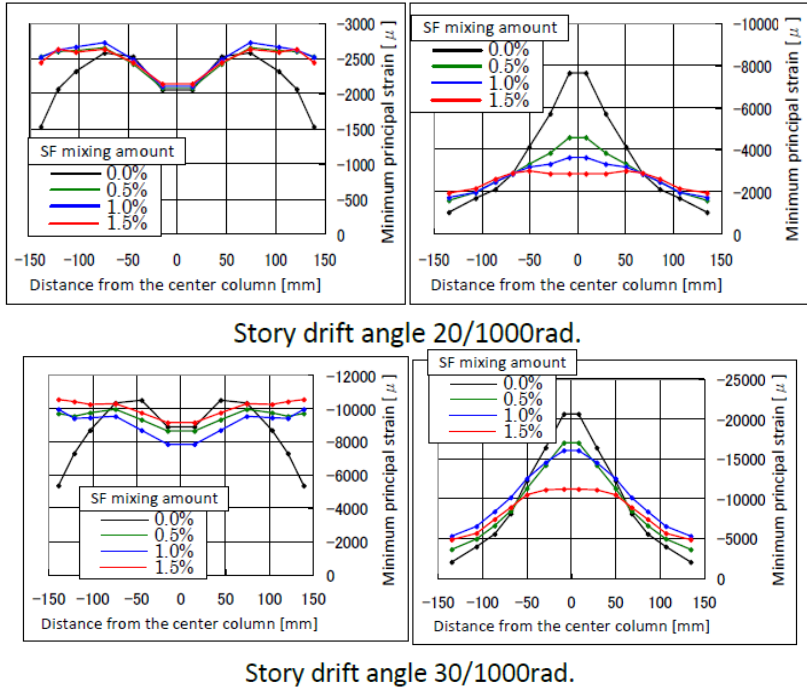
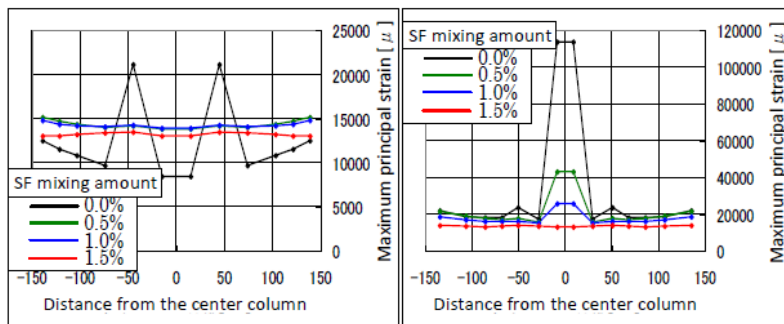


Fig. 8: Measuring element (Red frame)



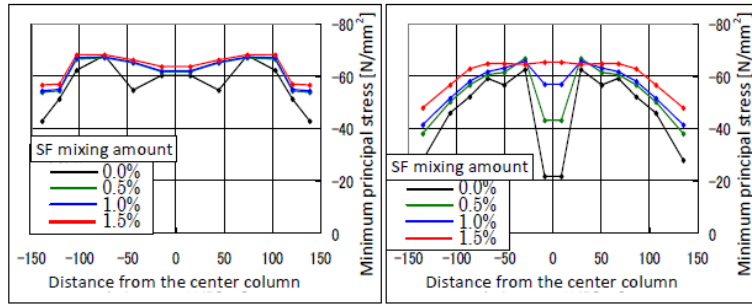
Story drift angle 30/1000rad.

Fig. 9: Minimum principal strain



Story drift angle 20/1000rad.

Fig. 10: Maximum principal strain



Story drift angle 20/1000rad.

Fig. 11: Minimum principal stress

### 3.6. Effective joint width and joint shear strength

The shear stress applied to each layer [Figure 12(b)], which shows a horizontal cross-section, was obtained from the shear stress measured at the joint center axis position (Figure 12(a), which shows a vertical cross-section). Figure 13 shows the distribution in the column-width direction at maximum resistance. The purple alternating long and short dashed line in Figure 13 indicates the effective joint width position obtained from the AIJ Design Guidelines [9].

The shear stress at the effective joint width position for the specimen without SF was obtained from the AIJ Design Guidelines [9]( $\tau_j'$  hereafter). It is assumed that the shear force is effectively borne at positions corresponding to  $\tau_j'$  or above. For specimens with SF, the sections corresponding to  $\tau_j'$  are obtained as effective joint widths. Figure 14 shows the rate increase relative to the specimen without SF. Lines where the effective joint width is deemed to be equal to the column width when the effective joint width exceeds the column width are referred to as "with limitation", and lines where the column width is not considered are referred to as "without limitation". The joint horizontal shear force at the center axis of the joint ( $V_j'$  hereafter) was obtained, which was in turn divided by the effective joint width (with restriction) and the column depth to obtain the joint shear strength. Figure 15 shows this as the rate increase expressed relative to the specimen without SF.

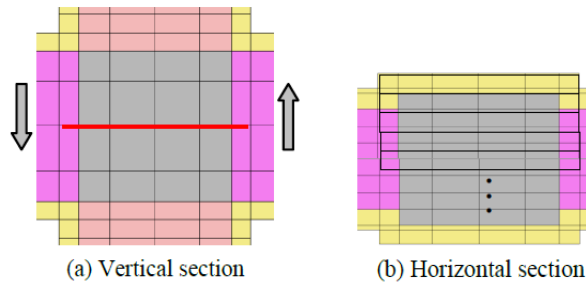
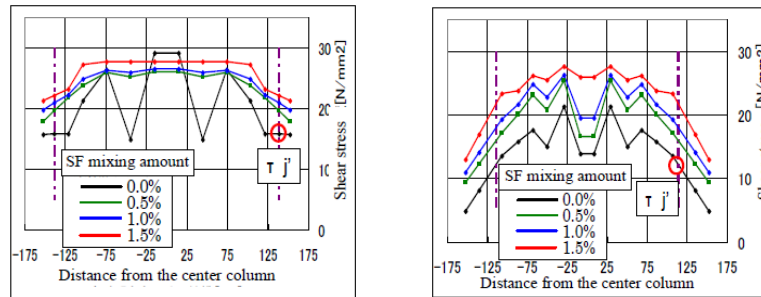


Fig. 12: Shear stress measurement position



Maximum strength

Fig.13: Shear stress (Left: 250-N series, Right: 152.5-N series)

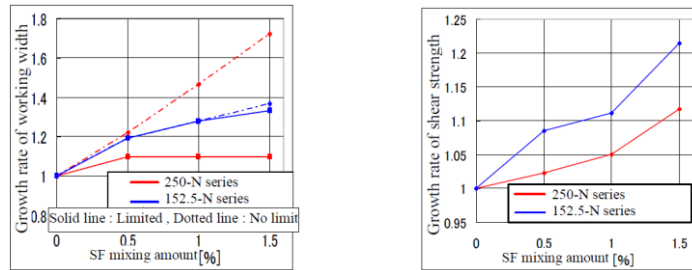


Fig. 14: Growth rate of width Fig. 15: Growth rate of shear strength

### 3.6.1. Increase in the effective joint width

The effective width increases as the SF content increases. In the 250-N series, the effective joint width already reaches the column width when the SF content is only 0.5%, and the effect of adding SF is not sufficiently exhibited.

### 3.6.2. Increase in joint shear strength

Similar to the effective width, the shear strength increases as the SF content increases. The shear strength rates of increase likely differ between the 250-N series and the 152.5-N series because the tensile principle strain within the joint for the 250-N series is almost as uniform as possible when the SF content is still 0.5%.

### 3.6.3. Effectiveness of SF in relation to the shear resistance in beam-column joints

Beam-column joints are believed to be effective when SF is added to concrete with a small beam width (effective joint widths) relative to the column width as the effective joint width should expand upon the addition of SF or in joints with localization of compressive characteristic degradation due to concrete cracking. As an example, in a beam-column joint where the beam joins the column with complete eccentricity, degradation of compressive characteristics due to concrete cracking is assumed to be localized because expansion of the effective joint width is exhibited only on one side. Hence, it is assumed that the increase in shear resistance due to the effect of SF is less than that in joint without eccentricity.

## 3.7. Stress distribution near the critical cross-section of the beam

Figure 16 shows the stress distribution at the critical cross-section of the beam with equal  $V_j$  and maximum resistance. The section above the center position of the beam is the compression side, while the section below is the tension side. For both series, the neutral axis in the specimen without SF is located below the center position, and compressive stress is present in all regions of the critical cross-section of the beam. In specimens with SF, the neutral axis is partially maintained towards the beam center, and tensile stress is present on the tension side. However, at the maximum resistance, the neutral axis is located further downward, and compressive stress is present in almost all regions, but the compressive force on the tension side is smaller than that in the specimen without added SF. Additionally, on the compression side, compressive stress is greater in specimens with SF.

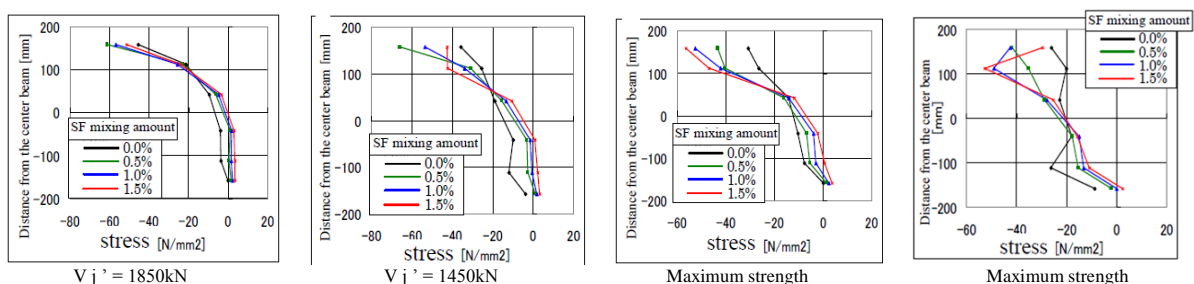


Fig. 16: Stress at critical section of the beam (Left: 250-N series, Right: 152.5-N series)

### 3.8. Proportion of shear force inputted into the joint

Figure 17 shows the stress conditions around the joint. Because tensile force is borne by concrete with added SF (section 3.7), the tensile force has to be considered. Equation (1) represents  $V_j'$  under these stress conditions. The portion underlined by line A indicates the input shear force from the concrete at the ends of the beam and column, while the portion underlined by line B represents the input shear force due to the bond force of the main beam reinforcement.

$$V_j' = \underbrace{[{}_bC_{cc} + {}_bT_c - {}_bC_{ct} - V_c]}_A + \underbrace{[{}_bT_s - {}_bC_s]}_B \quad (3.1)$$

$V_c$  : Column shear force,  ${}_bC_{cc}$  ( ${}_bC_{ct}$ ) : Compressive resultant force acting on concrete beam ends,  ${}_bT_c$  : Tensile resultant force acting on concrete beam ends,  ${}_bC_s$  : Steel compressive force,  ${}_bT_s$  : Steel tensile force.

Figure 18 shows the proportion of shear force inputted into the joint at equal  $V_j$  and maximum resistance. The shear force inputted into the joint is comprised of  $[{}_bT_s - {}_bC_s]$ , which is due to the bond force of the main beam reinforcement.  $[{}_bT_c]$  is the net beam end concrete tensile force on the tension side, and  $[{}_bC_{cc} - {}_bC_{ct} - V_c]$  represents all other components. The bond force of the main beam reinforcement is obtained from the difference in the main beam reinforcement force at the critical cross-section of the beam while the net beam end concrete tensile force on the tension side is measured from elements on the tensile side of the critical cross-section position of the beam. The other components are obtained by subtracting  $[{}_bT_s - {}_bC_s]$  and  $[{}_bT_c]$  from  $V_j'$ . In both series, adding SF causes the proportion of input shear force due to the bond force of the main beam reinforcement to decrease. The reason for the decrease is described based on Figure 17 when  $V_j'$  is constant according to Equation (1). As demonstrated in section 3.7, adding SF causes  ${}_bC_{cc}$  and  ${}_bT_c$  to increase, and  ${}_bC_{ct}$  to decrease. When this occurs, the value represented by the portion of Equation (1) underlined by line A increases. Because  $V_j'$  must be constant, the value represented by the portion underlined by line B decreases. Hence, the portion of the input shear force due to the bond force of the main beam reinforcement is thought to decrease.

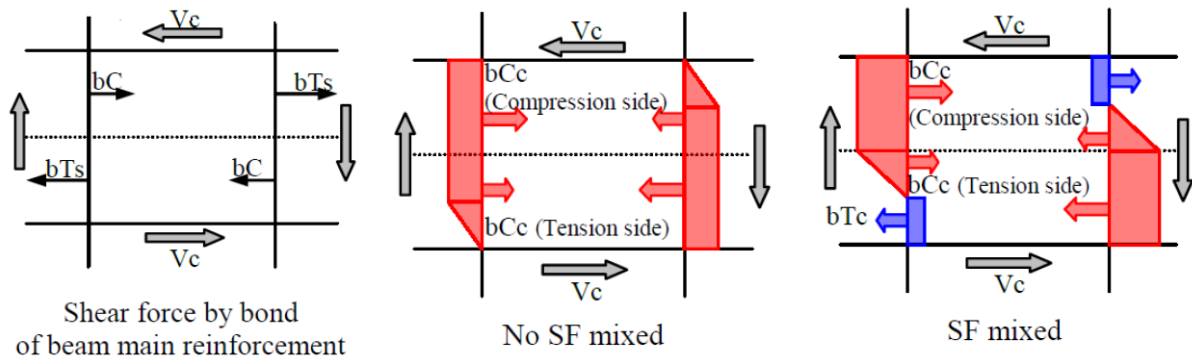


Fig.17: Stress near the joint

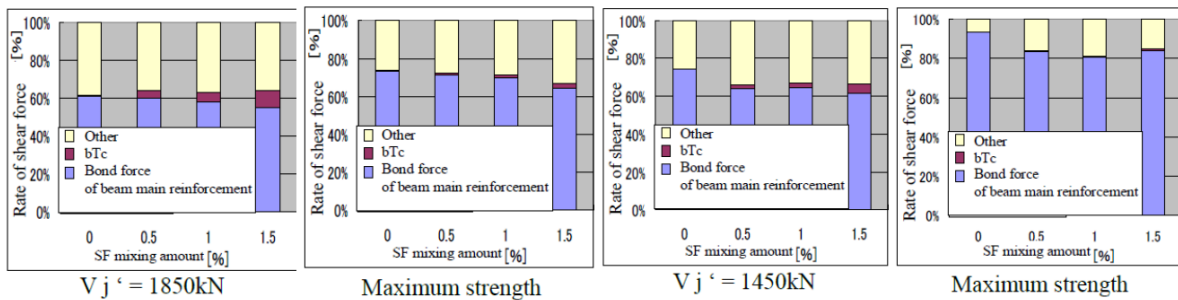


Fig. 18: Rate of joint shear force (Left: 250-N series, Right: 152.5-N series)

## 4. CONCLUSIONS

- (1) The increase in shear resistance in a beam-column joint due to added SF is a consequence of compressive stress transmitted as compressive struts in a uniform manner across the entire column-width direction in the joint, expanding the effective cross-section area of the compressive struts in the direction of column width.
- (2) Beam-column joints for which the addition of SF is believed to be effective in terms of shear resistance are those in which the beam width is small relative to the column width and concrete cracking is readily localized.
- (3) The tensile force in concrete must be considered to determine the joint input shear force of concrete containing SF.
- (4) The addition of SF causes the stress distribution at the critical cross-section of the beam to change, decreasing the proportion of shear force inputted into the joint as a result of bond force in the main beam reinforcement.

## ACKNOWLEDGEMENTS

The authors wish to express gratitude to Mr. Naoto Irisawa, a former graduate student of Chiba University. A part of this study was performed by N. Irisawa as partial requirement for the degree of MS. This study was conducted as a joint study with the Takenaka Research and Development Institute, Japan. The authors are grateful to Dr. Hideki Kimura, Mr. Atsushi Kanbayashi, Dr. Ousalem Hassane, Ms. Ai Yamada, and Dr. Takuya Kinoshita (Takenaka Corporation) for providing precious experimental data and sound advices.

## REFERENCES

- Takatsu H. and Kimura H. (2009). Experimental Study on Beam-Column Joint Using Steel Fiber Reinforced Ultra-High-Strength Concrete, *Proc. of the Japan Concrete Institute*, **31:2**, 559-564.
- Takahashi M., Sakashita T., Kashiwazaki T. and Noguchi H. (2009). Analytical Study on Steel Fiber-Reinforced Ultra High Strength Concrete Beam-Column Joints, *Summaries of Technical Papers of Annual Meeting, C-2*, Architectural Institute of Japan, 393-396.
- Sakashita T., Irisawa N., Kashiwazaki T., Noguchi H., Takatsu H. and Kimura H. (2010). Study on Aseismic Capacity of Steel Fiber-Reinforced Ultra High-Strength Concrete Beam-Column Joints by 3-D FEM Analysis, *Summaries of Technical Papers of Annual Meeting, C-2*, Architectural Institute of Japan, 449-452.
- Yo Y., Kashiwazaki T. and Noguchi H. (2005). 3-D FEM Analysis of Seismic Performance Evaluation of RC Columns Subjected to Reversed Cyclic Shear, *Proc. of the Japan Concrete Institute*, **27:2**, 157-162.
- Hong J., Kashiwazaki T. and Noguchi H. (2009). Study on Shear Strength of RC Beam-Column Joints by 3-D FEM Analysis, *Proc. of the Japan Concrete Institute*, **31:2**, 301-306.
- Kobayashi K., Mutsuyoshi H. (1980). Influence of Fiber Orientation and Distribution on Load-Deformation Characteristics of Steel Fiber Reinforced Concrete Members, *Proc. of the Japan Society of Civil Engineers*, **299**, 101-112.
- Sekiguchi Y., Kashiwazaki T., Noguchi H. and Takatsu H. (2010). Analytical Study on the Structural Performance of Ultra-High-Strength Fiber Reinforced RC Column, *Proc. of the Japan Concrete Institute*, **32:2**, 175-180.
- Tsuji D., Mitsui K., Kojima M. and Sugata M. (2008). Development of Fc200N/mm<sup>2</sup> Advanced Performance Composites : Part 2. Property of autogeneous shrinkage, bond stress of rebar and flexural toughness, *Summaries of Technical Papers of Annual Meeting, A-1*, Architectural Institute of Japan, 1089-1090.
- Architectural Institute of Japan (1999). Design Guidelines for Earthquake Resistant Reinforced Concrete Buildings Based on Inelastic Displacement Concept, Architectural Institute of Japan.